# Fusion of Drone and Satellite Data for Precision Agriculture Monitoring

Deepak Murugan*, Akanksha Garg*, Tasneem Ahmed†, and Dharmendra Singh*
*Department of Electronics and Communication Engineering
Indian Institute of Technology Roorkee, India-247667
†Department of Computer Application,
Integral University Lucknow-226026
Email: mdeepak.iitr@gmail.com, akanksha126@gmail.com, tasneemrke@gmail.com, dharmfec1@gmail.com

***Abstract*—In recent years, there is a strong need for large scale precision agriculture monitoring for improved productivity to meet the demands of growing population. At large scale, monitoring of agriculture precisely is a challenging task. Therefore, in this paper, a methodology has been proposed for precision agriculture monitoring i.e., to classify vegetation into sparse and dense vegetation classes by employing fusion of freely available satellite data (Landsat 8) and drone imagery. The methodology is able to successfully classify vegetation into the two classes and the results are verified with the help of drone image both visually, and quantitatively in the form of area estimation.**

***Keywords*—precision agriculture monitoring; drone; UAV; satellite images; SAM; Otsu thresholding**

## I. Introduction

Precision agriculture [1], [2] is being investigated for the past two decades and is still evolving with advancements in technologies. Drones or small unmanned aerial vehicles [3] are the latest addition to precision agriculture in recent years, rather than just being used for military purposes. Drones are available at affordable price and are capable of imaging ground data with its geographic locations. This helps the user to have a complete and clearer picture of the ground information. Multispectral camera equipped drones have taken the advantage of imaging the near infrared portion of the electromagnetic spectrum over the crops, which can provide the health condition of the crops. Utilization of drone images as an aid for information retrieval from satellite data for precision agriculture is an important area to be researched and needs to be explored.

Classification of land-cover [4] at major scale using satellite data has been carried out by many researchers. Some of the prominently used classification algorithms are decision tree [5], thresholding, support vector machine, neural network, object based image analysis (OBIA) [6] and time series analysis [7]. Most of the classification techniques are used to classify different classes like vegetation, water bodies, urban, bare soil etc. But within class classification such as classification of sparse and dense classes under vegetation class has not been explored much yet. Hyperspectral imagery [8] is generally used for similar type of classification like crop type mapping, wetland mapping etc., but these data are generally not available for all the geographic locations and has poor temporal resolution, which is an important aspect for large scale agriculture monitoring. Within class classification which is a part of precision agriculture monitoring is still a challenging and cumbersome task. This could be possible by information fusion of satellite data with drone imagery [9], as drone can provide precise ground truth information. But drone has to be used in such a way that its repetitive use can be minimized, to make it a cost effective solution.

In this paper, a methodology is proposed for identifying sparse and dense vegetation classes precisely in Landsat 8 data using drone data. Drone data has also been used for the verification of the obtained classified results, visually and by comparing the areas of both the identified classes with the areas computed using drone image.

## II. Study Area and Data Used

### A. Study area

The area where the drone images were acquired is located in the localities of Roorkee tehsil in the state of Uttarakhand, India. The study area selected for this work has a central latitude $29.93059655^0$ E and longitude $77.96395277^0$ N. Most of the area in the selected region is of agricultural land and sugarcane is one of the most cultivated crops. Other crops like rice and pulses were also cultivated during the period of July-August.

### B. Data used

Landsat 8 data having 11 spectral bands is chosen for this study and has a repeat cycle of 16 days. The tile data (Data ID: LC81460392016206LGN00), acquired on $24^{th}$ July 2016, covers the whole Haridwar district of Uttarakhand, India, along with some parts of neighboring districts.

Drone data acquired over the study area is another data used for this work. DJI phantom quadcopter with 4K resolution RGB camera is employed for this work. Images were acquired on $09^{th}$ August 2016 of a field with major crop as sugarcane and fallow land (bare field).

## III. Theoretical Background and Model Development with Implementation

The implementation procedure of the developed method along with its theory and results are described in the following sub-sections.

TABLE I
DETAILS OF LANDSAT 8 BANDS USED [10]

| Band No. | Wavelength (m) | Significance |
|---|---|---|
| 1 | 0.43 - 0.45 | Coastal and aerosol studies |
| 2 | 0.45 - 0.51 (Blue) | Detection of changes in chlorophyll / carotenoids ratios indicative of plant stress |
| 3 | 0.53 - 0.59 (Green) | Reflectance peak controlled by the presence of chlorophyll |
| 4 | 0.64 - 0.67 (Red) | Absorption by chlorophyll as well as tannin and anthocyanin |
| 5 | 0.85 - 0.88 (NIR) | Related to physical structure of mesophyll layer |
| 6 | 1.57 - 1.65 (SWIR 1) | Absorption due to leaf moisture content |
| 7 | 2.11 - 2.29 (SWIR 2) | Absorption due to leaf moisture content, foliar nitrogen and protein absorption |

### A. Drone data acquisition and preprocessing

Drone with a high resolution camera is flown over the study area at an altitude of 100 m. Series of images are captured at nadir view, with at least 40 percent overlap of two consecutive images captured. The captured images are then processed using ENVI Onebutton tool, which provides mosaicked, orthorectified and geo-registered image of the whole study area. Subset of drone image captured over the study area along with its some zoomed dense and sparse vegetation regions of sugarcane field are shown in Fig. 1(a,b,c) respectively.

### B. Landsat data preprocessing

Landsat 8 data has a total of 11 bands, out of which seven multispectral bands (band 1-7) having 30 m resolution are used in this work. Wavelength range of each band along with its land-cover specific importance is mentioned in Table I. NIR and SWIR mentioned in the table are near infra red and short wave infra red respectively.

The obtained data are stored as quantized and calibrated Digital Numbers (DN). The DN are converted to surface reflectance value using the equation (1) with coefficients provided in metadata file.

$$\rho = M_\rho . Q_{cal} + A_\rho \tag{1}$$

Where, $\rho$ is the spectral reflectance, $M_\rho$ is reflectance multiplicative factor from the band, $A_\rho$ is reflectance additive factor and $Q_{cal}$ is the pixel value in DN.

Once the surface reflectance of required bands are calculated, they are stacked to get one single image. In this work seven bands are layer stacked for further processing. Common area corresponding to drone image is segmented from the stacked Landsat image using the bounding co-ordinates. The true color and false color images of the subset area from Landsat 8 data are displayed in Fig. 1(d,e) respectively.

### C. Model development

The model that is developed for segregating vegetation into two classes is given in a stepwise procedure as follows,

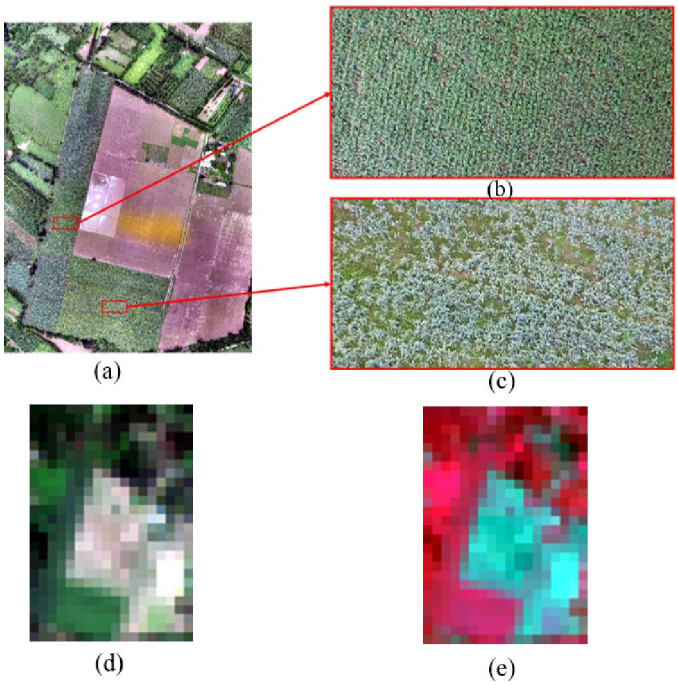


Fig. 1. Study area (Centre Latitude/Longitude- 29.93059655 E / 77.96395277 N) (a) drone image (b) dense sugarcane field (c) sparse sugarcane field (d) Landsat RGB (band 4,3,2) Image (e) Landsat FCC (band 5,4,3)

Step 1: Minimum noise fraction (MNF) transform is applied on the stacked Landsat image for dimensionality reduction. MNF is used to determine the inherent dimensionality of the image and it is performed using two cascaded PCA (Principal Component Analysis). The bands resulted after the MNF transformation are ranked based on the amount of variance. Rank of the bands decreases with decreasing variance until only noise and no coherent image is left.

Step 2: Pixel purity index (PPI) algorithm is then applied on MNF transformed image. The PPI algorithm identifies the most spectrally pure endmember from the image by projecting n-dimensional scatter plot onto random unit vector. The endmembers obtained from PPI algorithm are plotted which are shown in Fig. 2.

Step 3: Once the spectrally pure signatures are obtained, spectral angle mapper (SAM) is used to classify the image into several classes viz., water bodies, vegetation, urban and bare soil etc. The classified image obtained is shown in Fig. 3(a) where different colors represent different classes. Basically, SAM calculates the angle between the known pure endmember spectra and pixels. The pixels with angle less than a threshold limit against one of the endmembers are grouped into corresponding classes. In this study, a threshold of $10^0$ is chosen for the angles of pixels to be classified.

Step 4: The classified image of Fig. 3(a) is compared with the drone image for the identification of various classes. Classes that correspond to vegetation region are extracted from the classified image by creating a mask for rest of the classes as displayed in Fig. 3(b).

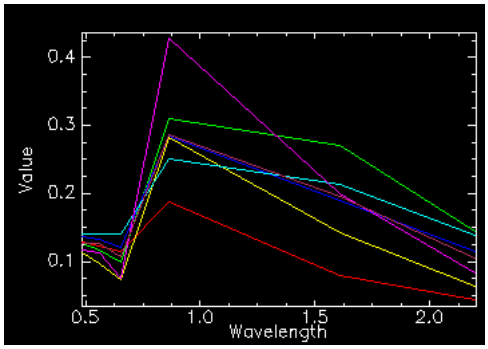


Fig. 2. Reflectance of spectral endmembers obtained from PPI algorithm

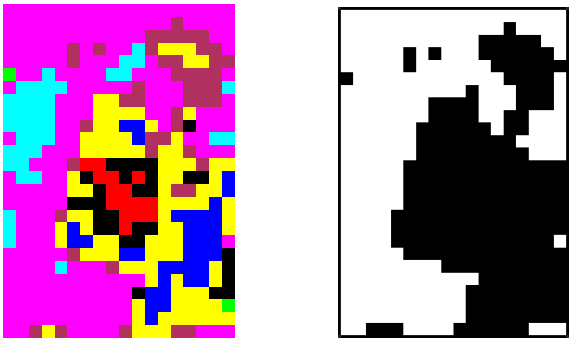

(a) (b)

Fig. 3. Subset area (a) SAM classified image (b) mask for vegetation extraction (white- vegetation, black- other classes)

TABLE II
GROUND TRUTH DATA STATISTICS AND SEPARABILITY INDEX (SI)

| Bands | Sparse | | Dense | | SI |
|---|---|---|---|---|---|
| | $\mu$ | $\sigma$ | $\mu$ | $\sigma$ | |
| Red | 0.078801 | 0.001366 | 0.082593 | 0.001789 | 1.19 |
| NIR | 0.380075 | 0.009078 | 0.384739 | 0.021102 | 0.15 |
| SWIR1 | 0.170956 | 0.002615 | 0.151363 | 0.005123 | 2.50 |
| SWIR2 | 0.069867 | 0.002426 | 0.061544 | 0.003603 | 1.36 |
| NDVI | 0.656403 | 0.009691 | 0.645748 | 0.019525 | 0.36 |

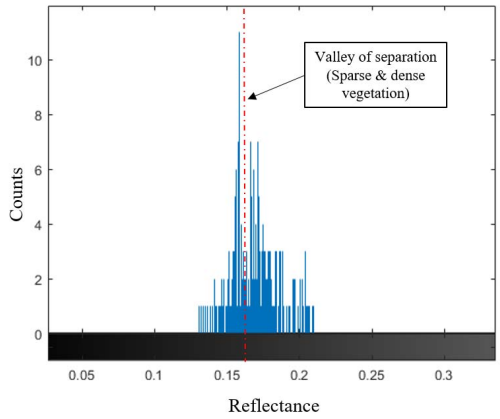


Fig. 4. Histogram of vegetation pixels of SWIR 1 band (band 6)

Step 5: The next step is to distinguish sparse and dense vegetation from the vegetation region obtained. Ground truth points are collected for both the classes separately from Landsat image with the aid of drone images.

Step 6: It is known that infrared bands provide better information regarding vegetation as compared to other optical bands. In order to determine the best band for separating the two classes in vegetation, separability index (SI) is used. Separability index [5] is given by equation (2),

$$SI_{i,j} = \frac{|\mu_i - \mu_j|}{\sigma_i + \sigma_j} \tag{2}$$

where $\mu$ and $\sigma$ are the statistical mean and standard deviation of classes i and j respectively. The separability index that lie between 0.8 and 1.5 indicates that the two classes are separable, SI greater than 1.5 indicates high separability and lower than 0.8 indicates both classes mix together in the selected spectral band. The separability index obtained for bands 4-7 and normalized difference vegetation index (NDVI) are shown in Table II. Hence, it is clear from the table that SWIR1 (band 6) has better separability for sparse and dense vegetation regions as compared to the other bands.

Step 7: Once the band is selected to classify the two classes using SI, proper threshold value is to be selected for better segregation. Mean computed using the collected ground truth points from Landsat data with the aid of drone imagery is tabled in Table II, and is used as an initial point for obtaining the threshold value. Shown in Fig. 4 is the histogram of vegetation pixels obtained by applying vegetation mask over band 6. It has been observed that there exists a valley between the two selected classes and it supports our finding on separability as well.

Otsu thresholding [11], a popular global automatic threshold is selected to determine the threshold value for classification of the two classes. Let the number of gray levels present in the images be $L$ $[1, 2, 3, \cdots, L]$. The image is classified into two classes $C_0$ $[1, 2, \cdots, k]$ and $C_1$ $[k+1, k+2, \cdots, L]$, where k is the threshold gray level. Otsu method selects optimal threshold that maximizes the discrimination criteria ($\eta$) as mentioned in equation (3) which in turn maximizes the variance ($\sigma_B^2$) between the two classes as in equation (4).

$$\eta(k) = \sigma_B^2(k)/\sigma_T^2 \tag{3}$$

$$\sigma_B^2 = \omega_0\omega_1(\mu_1 - \mu_0)^2 \tag{4}$$

$$\sigma_T^2 = \sum_{i=1}^{L}(i - \mu_0)^2 p_i \tag{5}$$

where $\omega_0$ and $\omega_1$ are the probabilities of class occurrence, $\mu_0$ and $\mu_1$ are the respective class mean levels and $\sigma_T^2$ is the total variance level. Threshold value is obtained by applying Otsu method on the intensities that lie between the mean values of the two classes. Then the image is classified into

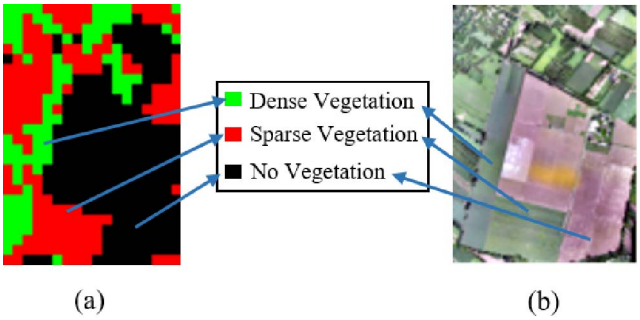


Fig. 5. (a) Landsat 8 subset classified into sparse and dense vegetation (b) Drone image

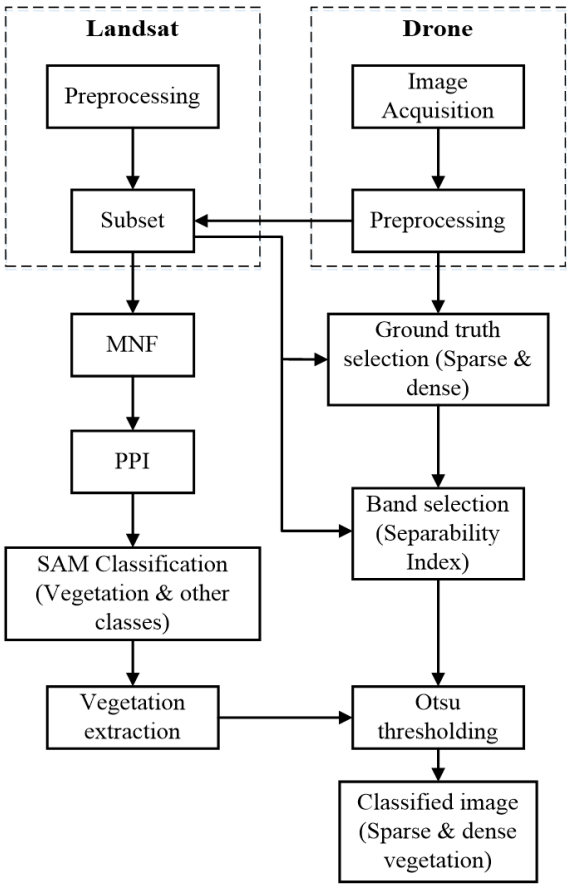


Fig. 6. Flowchart of the proposed methodology

sparse and dense vegetation classes by using the obtained threshold as shown in Fig. 5.

Step 8: Approximate area estimates for sparse and dense vegetation classes have been computed for Landsat image and drone image, and are tabled in Table III. In case of drone image, areas have been computed by drawing polygons for all the sparse and dense vegetated fields. While comparing from the table, it has been observed that there is very less difference between the areas obtained using the two images.

Complete flowchart of the proposed methodology is shown in Fig. 6.

TABLE III
AREA ESTIMATION

| Class | Area computed by Landsat image (sq. km approx.) | Area computed by Drone image (sq. km approx.) |
|---|---|---|
| Sparse vegetation | 0.1386 | 0.1109 |
| Dense vegetation | 0.0810 | 0.1364 |
| Vegetation region | 0.2196 | 0.2473 |
| Other regions | 0.2016 | 0.1782 |
| **Total** | **0.4212** | **0.4255** |

## IV. DISCUSSION

In this paper, Landsat image has been classified (Fig. 3(a)) into vegetation and other classes by SAM classifier using spectral endmembers obtained from PPI. Ground truth data is also extracted from Landsat data with the help of drone image for the two classes; sparse and dense vegetation. Band 6 (SWIR 1) is chosen for classification by utilizing separability index as mentioned in Table II. Otsu thresholding is employed to determine the optimal threshold value between mean values of the two classes (sparse and dense vegetation). Then the extracted vegetation pixels are classified into the two classes using the obtained threshold value. The classified image obtained (Fig. 5) has been verified visually by overlaying onto the drone imagery (Fig. 1(a)), and also validated by comparing the areas of the two classes of the former image with that of the obtained using later image. Approximately, equivalent areas are obtained for both the classes, as given in Table III. But it can also be observed from the table that there is a significant decrease in the area of dense vegetation in the Landsat image as compared to drone image, and this is due to the presence of mixed pixels that contain dense vegetation along with sparse and/or other classes and has been classified into one of the other classes. Hence, it is evident that the methodology is able to perform good classification.

## V. CONCLUSION

In this paper, a methodology based on fusion of drone image and optical satellite data has been proposed for precision agriculture monitoring. It opens up the prospects for within class classification i.e., classification of sparse and dense vegetation, which is an important aspect for precision agriculture monitoring. The proposed algorithm proves to be successful in distinguishing the two vegetation classes, or precision agriculture monitoring, and the same is validated by comparing the Landsat classified image with the drone image. In future, this methodology can also be automated by the utilization of drone with multispectral imaging capability and also employment of sub-pixel analysis technique for improved area estimation.

## ACKNOWLEDGMENT

Authors are thankful to RailTel, and ICAR (Indian Council of Agricultural Research), India for providing the funds to support this work.

## REFERENCES


[1] D. J. Mulla, "Twenty five years of remote sensing in precision agriculture: Key advances and remaining knowledge gaps," *Biosyst. Eng.*, vol. 114, pp. 358–371, Apr. 2013.

[2] A. McBratney, B. Whelan, T. Ancev, and J. Bouma, "Future Directions of Precision Agriculture," *Precis. Agric.*, vol. 6, pp. 7–23, Feb. 2005.

[3] C. Zhang and J. M. Kovacs, "The application of small unmanned aerial systems for precision agriculture: a review," *Precis. Agric.*, vol. 13, pp. 693–712, July 2012.

[4] D. Lu and Q. Weng, "A survey of image classification methods and techniques for improving classification performance," *Int. J. Remote Sens.*, vol. 28, pp. 823–870, Mar. 2007.

[5] P. Mishra and D. Singh, "A Statistical-Measure-Based Adaptive Land Cover Classification Algorithm by Efficient Utilization of Polarimetric SAR Observables," *IEEE Trans. Geosci. Remote Sens.*, vol. 52, pp. 2889–2900, May 2014.

[6] T. Blaschke, "Object based image analysis for remote sensing," *ISPRS J. Photogramm. Remote Sens.*, vol. 65, pp. 2–16, Jan. 2010.

[7] Y. Shao, R. S. Lunetta, B. Wheeler, J. S. Iiames, and J. B. Campbell, "An evaluation of time-series smoothing algorithms for land-cover classifications using MODIS-NDVI multi-temporal data," *Remote Sens. Environ.* , vol. 174, pp. 258–265, Mar. 2016.

[8] M. Govender, K. Chetty, and H. Bulcock, "A review of hyperspectral remote sensing and its application in vegetation and water resource studies," *Water SA*, vol. 33, Jan. 2007.

[9] C. Gevaert, "Combining hyperspectral UAV and mulitspectral FORMOSAT-2 imagery for precision agriculture applications," *LUMA-GIS Thesis*, 2014.

[10] J. Townshend, C. Justice, W. Li, C. Gurney, and J. McManus, "Global land cover classification by remote sensing: present capabilities and future possibilities," *Remote Sens. Environ.*, vol. 35, pp. 243–255, Feb. 1991.

[11] N. Otsu, "A threshold selection method from gray-level histograms," *Automatica*, vol. 11, no. 285-296, pp. 23–27, 1975.